NANO LETTERS

2006
Vol. 6, No. 12
2790−2796

Fringing Field Directed Assembly of Nanomaterials

Chad R. Barry and Heiko O. Jacobs*

Department of Electrical and Computer Engineering, University of Minnesota, 200 Union Street SE, Minneapolis, Minnesota 55455

Received August 9, 2006; Revised Manuscript Received October 11, 2006

ABSTRACT

This letter reports on a new gas-phase printing approach to deposit nanomaterials into addressable areas on a surface with 50 nm lateral accuracy. Localized fringing fields that form around conventional resist patterns (PMMA and SiO2) with openings to a silicon substrate are used to direct the assembly of nanomaterials into the openings. Directed assembly was observed due to a naturally occurring inbuilt charge differential at the material interface that was further enhanced by corona charging to yield a field strength exceeding 1 MV/m in Kelvin probe force microscopy (KFM) measurements. The assembly process is independent of the nanomaterial source and type: an evaporative, plasma, and electrospray source have been tested to deposit silicon and metallic nanoparticles. The results suggest a potential route to form nanolenses on the basis of charged resist structures; a 3-fold size reduction has been observed between the structures and the assembled particles. Applications range from the integration of functional nanomaterial building blocks to the elimination of lift-off steps in semiconductor processing.

The ability to print, deposit, or assemble nanomaterials in two and three dimensions will enable the fabrication of a whole range of novel devices. There is a distinction to be made between the first-generation devices that are formed by patterning films and nanomaterials using conventional lift-off and etching techniques and the second-generation devices that require a localized order, placement, and formation of interconnects on a single nanocomponent (nanoparticle or nanowire) basis. Current examples of the second-generation devices that require interconnects and/or localized order of single components include single-nanocomponent transistors,[1−3] light-emitting diodes, lasers,[4] sensors,[5] passive photonic networks,[6] or nanoparticle based media for data storage.[7] New technologies that can deliver and integrate single components at precise addressable locations on a surface are needed to enable the manufacturing of the second-generation devices. Most recent research has focus on concepts that are based on directed self-assembly and template-assisted assembly,[8,9] exploring a variety of different forces including hydrophobicity/hydrophilicity,[10] magnetic interactions,[11] electrospinning,[12] microfluidics,[13] and electrostatics or coulomb forces.[14−21] Interestingly most of these concepts, except those using electrostatics[14−18] and electrospinning,[12] are exclusive to the assembly from the liquid phase. Liquid-phase concepts, considering solution chemistry as the nanomaterial source, are important; however, an equally large amount of functional nanomaterials are formed using gas-phase methods. The semiconductor industry for example uses gas-phase synthesis and deposition techniques exclusively when high-performance materials (conductors, semiconductors, and insulators) are needed. While the materials are often considered to be of better quality, there are a number of limitations: patterning by etching and lift-off waste materials, the resolution is limited by the resist pattern, and randomness is observed in the deposition patterns if discrete nanoparticles or nanowires are deposited.

This communication presents a new directed assembly process that can be attached in a modular form to existing[14,16,22,23] gas-phase systems. The approach is different from prior nanoxerographic printing methods that use continuous dielectric film layers. The primary aim of the approach is to direct single nanoparticles into addressable regions on a surface with sub-100 nm control over the position. It is an additive process that directs the material into target locations, conserving material and eliminating lift-off or etching steps. The process works at atmospheric pressure and intermediate vacuum (10^{-4} Torr) and employs a carrier gas that transports charged nanomaterials from a reactor into an assembly module. It combines Coulomb force directed assembly[16−18] with topographically patterned materials that can be formed by conventional lithography.

Figure 1 illustrates the gas-phase nanomaterial deposition concept. A global (E_G) and localized (E_F) electrostatic fringing field is used to direct the assembly of charged nanomaterials into micro- or nanometer sized openings. The assembly occurs inside a 1 cm tall insulating channel with an inlet and outlet on either side that holds two 1 cm × 1 cm squared top and bottom copper electrodes. The fringing field is formed using a charged, patterned thin film on top

* Corresponding author. E-mail: hjacobs@umn.edu.

10.1021/nl0618703 CCC: $33.50
Published on Web 10/27/2006

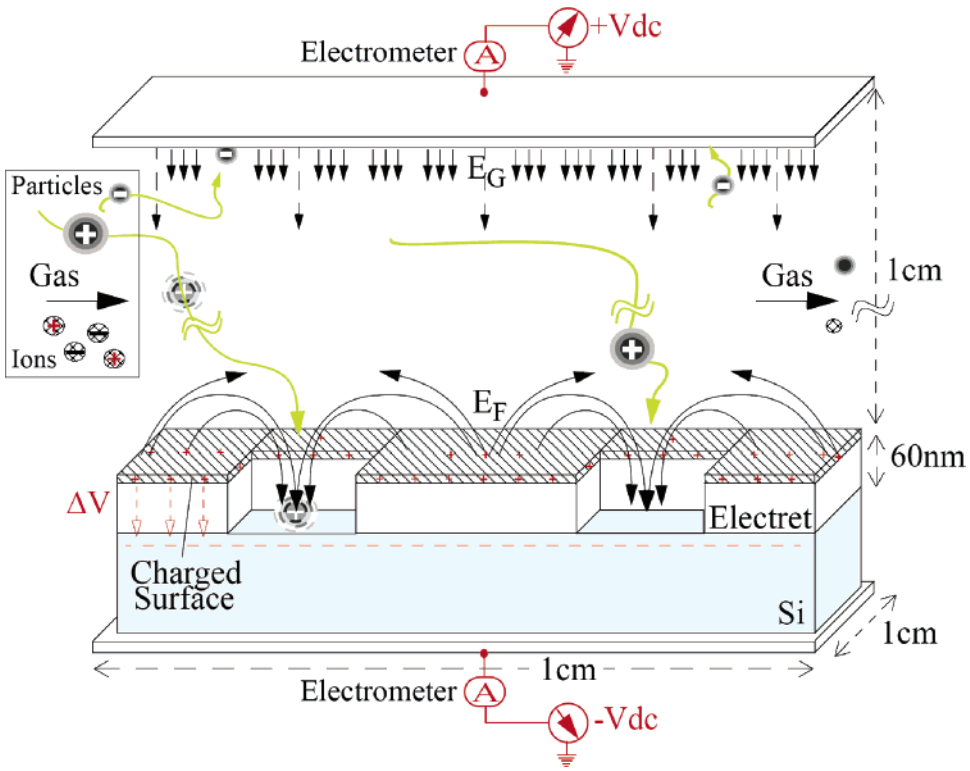

Figure 1. Illustration of the sample and assembly module. A carrier gas delivers charged nanoparticles and ions. A global field E_G directs charged particles of selected polarity toward the charged sample surface, establishing an electrometer current. A potential ΔV is present between the electret and substrate. The potential gives rise to local fringing fields E_F that direct nanoparticles into the openings.

of a silicon chip. The surface of the electret is at a different electrostatic potential than the silicon chip. Electrostatic field lines are present not only inside the electret but also outside, affecting the nanoparticle trajectories. The line integral $\int \boldsymbol{E}_F \, d\boldsymbol{l} = \Delta V$ relates the strength of the fringing field (E_F) with the potential difference (ΔV) between the charged electret surface and the substrate. The externally biased electrodes select and direct incoming particles of a desired polarity toward the chip surface. Both electrodes are connected to an electrometer (Keithley 6517A) to monitor the current and charge that arises when charged nanomaterials or ions deposit on the surface. In this Faraday cup arrangement, image charges flow from the ground through the electrometer into the sample or electrode plate to the location of assembled material. As a result, the electrometer measures the accumulated charge and subsequent current of the assembled particles or ions regardless of where they deposit on the surface or whether they become neutralized by the image charges. The deposition rate onto the plates inside this assembly module depends on the volume number concentration of charged nanomaterials and ions, gas flow, actual potential difference between the two plates, and pressure. It can be adjusted ranging from 3 pA at ultralow concentrations to 1 nA at high concentration.

As a nanoparticle source, we have tested three different systems, an evaporative,[16] electrospray,[22] and plasma[23] system, to create metallic and semiconducting nanoparticles (10−50 nm in size). The evaporative and electrospray system outlets are connected to the assembly module through a 1 cm diameter, 15−20 cm long Tygon tube. A mixture of CO_2 and compressed air with flow rates of 300 and 800 sccm, respectively, are used as carrier gases in the electrospray system to transport the nanomaterials into the assembly module. A 1500 sccm flow of argon is used in the evaporative system.

As electrets, we used SiO_2 or PMMA resist patterns with openings to a Si substrate. The patterns can be generated by any number of lithography methods. In our experiments, we used standard photolithography for large scale features (>10 μm) and electron beam (e-beam) or nanoimprint lithography for small scale features (≤1 μm). The large scale features were 15 μm square holes in 100 nm thick thermally grown silicon dioxide on a p-type silicon substrate. The holes were formed by standard lithography and reactive ion etching and not treated any further. The high-resolution samples consisted of 100 nm to 1 μm wide holes and lines in a 60−80 nm thick layer of PMMA (2% 950 K in chlorobenzene) that was spin-coated onto an n-type silicon wafer. The patterns were defined using electron beam lithography and developed in a 3:1 solution of IPA (isopropyl alcohol)/MIBK (methyl isobutyl ketone) for 40 s.

Both SiO_2 and PMMA on silicon exhibited an inherent built-in potential ΔV that can be changed by additional surface treatments. The potential ΔV that gives rise to the fringing fields is the key parameter in the self-assembly process. We have directly measured these potentials as a function of processing conditions using Kelvin probe force microscopy (KFM).[24] KFM is an atomic force microscopy based tool that can detect variations in the surface potential distribution with 100 nm scale lateral resolution and 5 mV

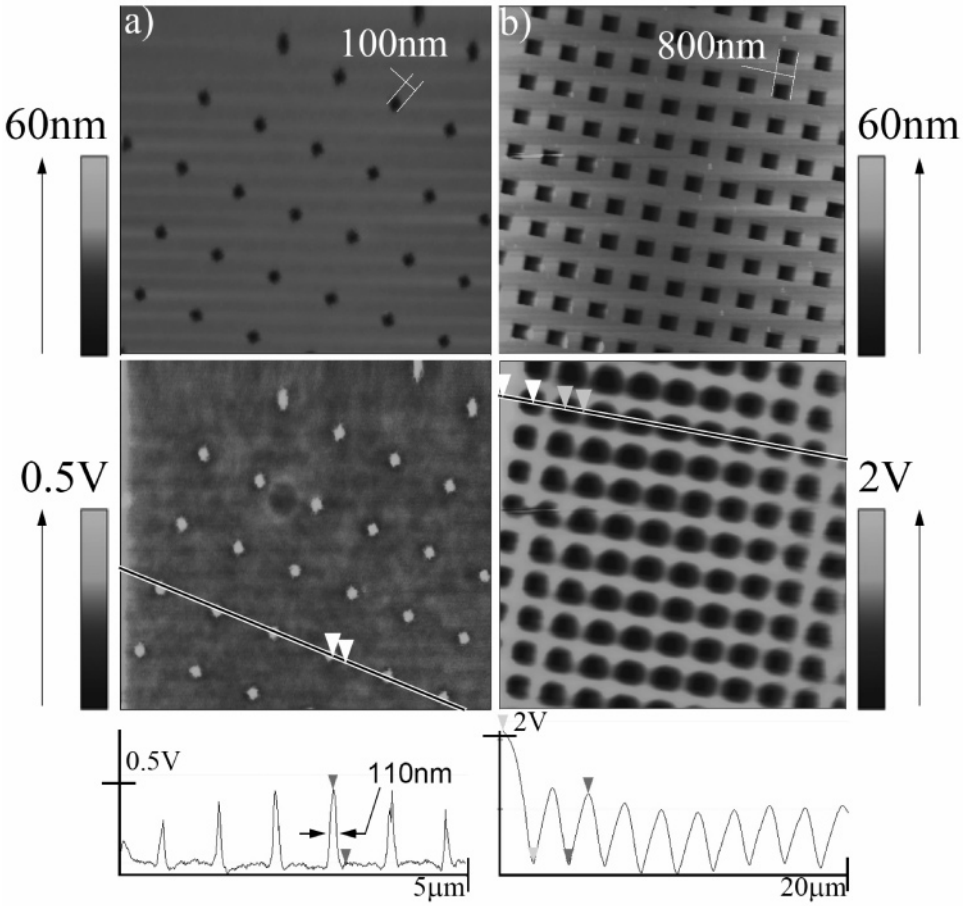

Figure 2. (top) Atomic force microscopy topographical images of the nanostructured PMMA and (bottom) corresponding surface potential images. (a) Sample charged during the electron beam lithography process. (b) Corona-charged sample.

sensitivity. Figure 2 illustrates an example of the change in surface potential difference between PMMA thin films and exposed silicon areas after different processing steps: (a) electron beam lithography and (b) corona charging. Figure 2a shows a 60 nm thick PMMA film on top of an n-type silicon wafer with a native oxide after e-beam exposure, development in MIBK, rinsing in IPA, and blow drying under a stream of dry nitrogen. The film contains 100 nm diameter holes and a 500 mV potential difference. As a qualitative statement, we rarely observed charge or potential differentials between dissimilar surface regions that are zero. The observation of a charge differential is the norm rather than the exception and has been used as a material contrast mechanism since 1997.[25] The charge differential between the patterned PMMA thin films and the underlying native oxide varied with the processing conditions. Silicon without native oxide did not show a strong charge differential (recorded values were smaller than 100 mV), which leads to the conclusion that the native oxide plays an important role. Our current hypothesis is that the PMMA is highly negatively charged during e-beam exposure, yielding a positive image charge in the silicon and native oxide layer underneath that could remain partially present after developing the PMMA in MIBK. We were able to remove >90% of the charge by dipping the chip in a 2% solution of HF in water for 30 s, which supports this hypothesis. However, other mechanisms such as charging by contact and friction when rinsing the dissimilar surfaces (PMMA and native silicon) with MIBK, IPA, and blow drying under a stream of dry nitrogen cannot currently be excluded.

Moreover, the recorded potential difference can be reversed or enhanced by a number of different methods, including a previously published concept[15,16] in which externally biased conformal electrodes are used to establish an electrical contact with the electret surface to reverse the potential. We tested this approach and obtained a potential difference of 500 mV for the 60−80 nm thick PMMA film. These potentials show greater stability, suggesting that the charge is embedded inside the PMMA film.

Figure 3 shows a new charging method that was used to create the 2 V potential difference in Figure 2b. The approach combines patterned electrets on conducting substrates with corona charging. A home-built corona charger, loosely based on work by Whitby et al.,[26,27] was used and connected to the particle assembly module. Argon gas was flowed (1000 sccm) through the charger and ionized using a positive DC corona discharge by applying a positive (2.5 kV) potential between the stainless steel needle and metal encasement. A fraction of the argon ions were carried away by the gas flow into the assembly module. We measured these ions inside the assembly module using the electrometer, which recorded negative 48 nC of accumulated charge on the positively

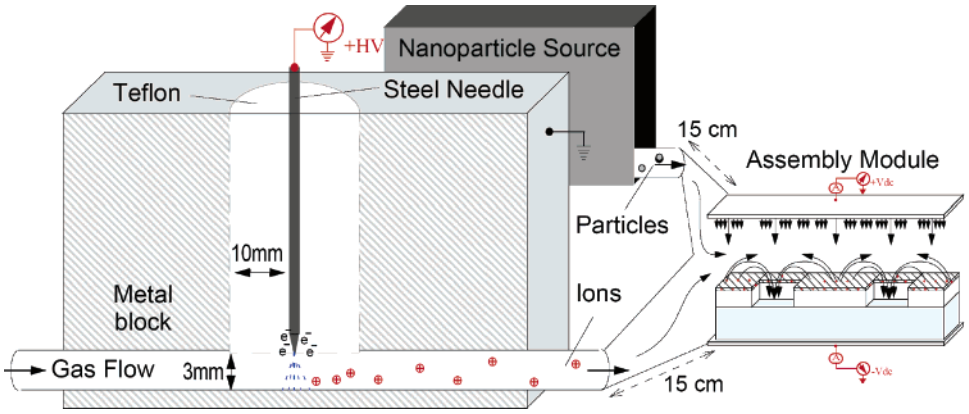

Figure 3. Inline corona charger. A high voltage is applied to an insulated needle positioned 3 mm away from a grounded metal tube. The induced electric field creates a corona region where ions are repelled from the needle and carried away by the carrier gas to the assembly module.

biased (100 V) top plate and a positive 360 nC of charge on the negatively biased (−100 V) bottom plate after 20 min of charging. A partial amount of the positive Ar ions are trapped on or inside the insulating electret surface, whereas the conducting silicon surface remains less affected. This approach was very successful; it yielded high potential differences exceeding 2 V (Figure 2b) between the nanostructured PMMA layer and semiconducting substrate. The observed 2 V potential difference for the corona-charged samples exceeds to the best of our knowledge any previously reported values for PMMA thin films of similar thickness. We attribute the broadening in the highly corona-charged samples to be dominated by repulsive Coulomb forces and charge diffusion instead of tip-related convolution. The charge retention time varied greatly with electret material, charging method, humidity, and storage container. Qualitatively, thermally grown silicon oxide did not retain its charge as well as PMMA and frequently lost most of its charge within less than 5 h. Electric contact-charged PMMA yielded superior retention times but lower charge differentials than corona-charged samples. All electrets (SiO_2 and PMMA), independent of the charging methods, retained a sufficiently large charge differential to conduct successful assembly experiments for several hours.

Figure 4 shows the first assembly attempt using a 30 μm pitch that illustrates the importance on balancing the strength of global and local fields. In theory, perfect assembly could be accomplished without any particles depositing on the resist structures if the local fields are strong and the global field is zero. The assembly would be largely independent of the pitch or layout of the pattern. The problem, however, is that the assembly process would not proceed very quickly; a small global field is needed to direct nanomaterials to the surface and the superposition of the two contributions has to be considered. Particles can and will end up in undesired areas on the resist structures if the empty areas exceed a certain threshold. In the illustrated experiment, we used a patterned SiO_2 substrate positively charged by electric contact charging with a flat gold-coated PDMS stamp.[15] The surface potential difference was measured by KFM to be $\Delta V = 300$ mV. A global electric field strength E_G of 20 kV/m (+200 V top electrode, −200 V bottom electrode) was used to initially direct the incoming particles.

The field on the silicon dioxide surface can be approximated to be $E_s = \Delta V/(\pi r) - E_G$ by considering simple parallel lines and half-circular field lines with radius r. This is a crude estimate that is only valid for a single-step potential, but it provides important insights into the basic principle. For example, it allows us to calculate a turning point $r_t = \Delta V/(\pi E_G)$, where the local field on the PMMA surface is equal to the global field. Beyond this turning point, particles will deposit on top of the resist structures. In the given case, the calculated value for r_t is ∼5 μm; the actual experimental values ranged from 5 to 7 μm. Another distinctive element is that the 15 μm openings are partially empty, resulting in focused assembly toward the center. The positively charged gold nanoparticles shown in Figure 4 were 10−100 nm in size and generated by evaporation, nucleation, and condensation within a tube furnace and carried to the particle assembly module in a 1.5 L/min flow of argon.[16]

Figure 5 shows high-resolution patterns, where the focusing effect becomes much more prevalent. The pitch has been reduced when compared to Figure 4. As long as r_t is larger than the actual pitch of the patterns, we find no particles on the PMMA coated areas. The openings create attractive funnels for particles to assemble into the holes that are largely independent of the pitch. Parts a and b of Figure 5 depict 10−40 nm silver nanoparticles created in the evaporative furnace system and assembled into ∼100 nm sized holes in corona-charged PMMA. By analyzing 130 holes, we derived the standard deviation from the center location to be ∼25 nm. The assembly parameters were as follows: 1500 sccm argon gas, atmospheric pressure, 1080 °C furnace temperature, 200 V global applied potential, 3 nC recorded charge accumulation, and 10 min assembly duration. Figure 5c shows gold colloids that have been assembled into the center of 300 nm wide trenches. A full width at half-maximum resolution of ∼75 nm was found by analyzing the 770 particles assembled in the three central lines of Figure 5c. The gold colloids were assembled using an electrospray system[22] that has been published previously. A 14μM suspension of 50 nm colloidal gold particles in water (BB

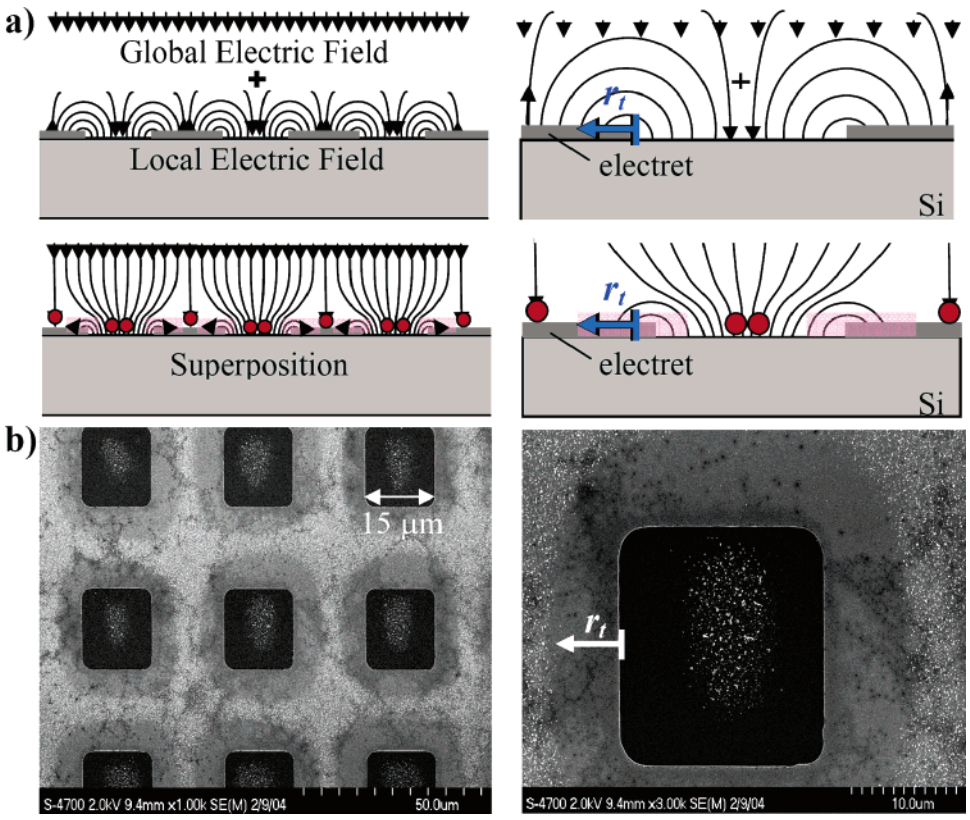

Figure 4. (a) Conceptual picture and (b) experimental result illustrating the effect of the global potential on the size of the empty areas. A 10 μm wide empty belt is visible. Holes are 15 μm wide.

International) was electrosprayed as received from the manufacturer without any alterations. The experimental parameters were as follows: a mixture of 300 sccm CO_2 and 800 sccm compressed air carrier gas, atmospheric pressure, ~100 nA electrospray current, 200 V global applied potential, 270 nC recorded charge accumulation, and 1.5 h. assembly duration. The longer assembly time for this process can be attributed to low solution concentration and low charge concentration on the particles due to the presence of a polonium 210 neutralizer.[22] Figure 5d shows 40 nm silicon nanoparticles that have been created in a constricted, filamentary, capacitively coupled, low-pressure plasma system.[23] Particles in this system were charged and we were able to extract them from the flow. There is ~6 orders of magnitude lower pressure in this system than in the evaporation and electrospray system. While we have been able to assemble the particles, the repeatability is not as consistent when compared to systems that deliver particles at atmospheric pressure. The primary reason points to a specific design problem. The plasma-generated particles enter a lower pressure chamber at high speeds (50−70 m/s)[28] and reach a nanoparticle assembly module with greater variations in the kinetic energy distribution. The estimated retained energy is at least 1 order of magnitude higher than the thermal energy in an atmospheric pressure system.

The observed focusing effect and expected precision can be studied by solving Langevin's equations of motion of nanoparticles inside an electric field. To establish an analytical form for the relative precision, we investigated a single particle at a radial distance r from the center of a patterned hole, as illustrated in Figure 6. In this case, the uncertainty acquired in the particle trajectory (Δr) due to Brownian motion can be described by the root-mean-square displacement or half-width of the Gaussian bell curve $\Delta r = \sqrt{2\Delta tD}$, where Δt is the time for a particle to deposit, $D = C{\cdot}kT/3\pi d\eta$ is the Stokes−Einstein diffusion coefficient for nanoparticles of diameter d, viscosity η, and empirical slip correction factor C. Maximum deviation considering a Newtonian trajectory will occur at the center, where the field strength is smaller and where the time to deposit will be increased. The electric field along the central particle path, $E_s = \Delta V/\pi r$, will cause the particle to follow the trajectory with a terminal velocity $v_t = C{\cdot}qE_s/3\pi d\eta = qE_sD/kT$. Substituting $\Delta t = r/v_t$ yields a normalized half-width of the Gaussian bell curve in the form:

$$\frac{\Delta r}{r} = \sqrt{2kT/qrE_s} = 2.507\sqrt{kT/q\Delta V} \qquad (1)$$

Equation 1 provides a number of important insights into electric-field-directed self-assembly processes. First, the key measure of the expected focusing will be the potential difference between charged and uncharged areas. Values of $q\Delta V$ larger than kT are desired. Second, the relative precision is independent of the size of the pattern and therefore scaleable. Third, the precision can be increased by increasing the particle charge. There are a number of other interesting points to make that are somewhat counter intuitive. Even though slip correction factors have been considered in the discussion, the precision seems to not directly depend on

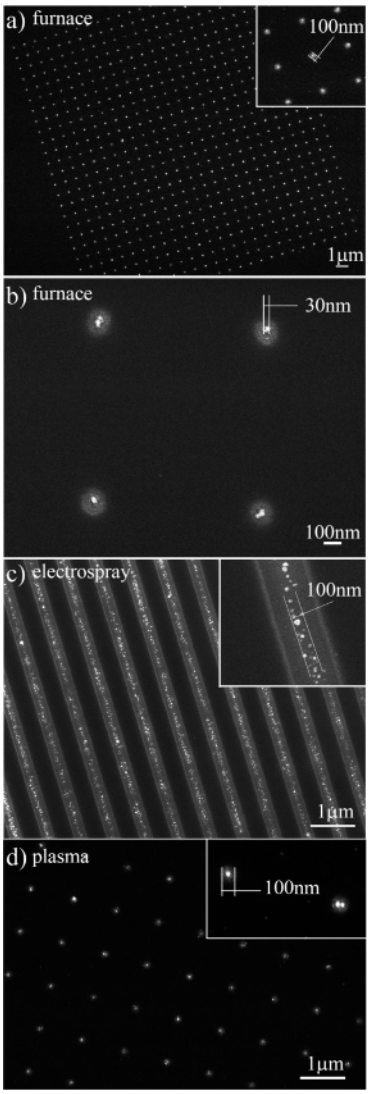

Figure 5. Nanoparticle assembly into holes and lines. (a,b) Silver nanoparticles focused into the center of ~100 nm holes from the evaporative furnace system. (c) 50 nm colloidal gold particles focused along the central area of 300 nm wide lines from the electrospray system. (d) 40 nm cubic silicon particles assembled into 100 nm holes from a capacitively coupled plasma system.

particle size. Parameters such as viscosity and pressure are also not present in the derived equations, suggesting that assembly at different pressures with different terminal velocities, collision frequencies, or mean free paths might be possible as well. Equation 1 is in good agreement with the range of precisions found experimentally. The measured values for ΔV ranged from 0.5 to 2 V. Nanoparticles in the thermal evaporation system are charged due to thermal ionization or thermionic electron emission with a typical charge value of 2 elementary charges for a 10 nm size particle and up to 35 elementary charges for a 100 nm sized particle.[29] The electrospraying system involves the use of a polonium 210 α radiation particle neutralizer, thereby leaving the particles predominantly singly charged.[30] Considering the full range from 1 to 35 elementary charges and 0.5−2 V potential yields a relative precision range $\Delta r/r$ from 5 to 57%.

In conclusion, we have developed a new gas-phase integration process to assemble nanomaterials into desired

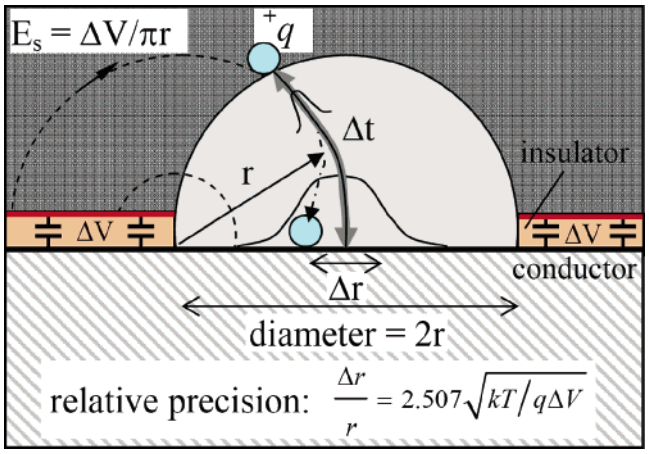

Figure 6. Graphical representation of the relative nanoparticle assembly precision ($\Delta r/r$), which was found to only be a function of the thermal energy (kT), the particle charge (q), and the surface potential difference (ΔV).

areas using localized fringing fields. We expect this process to work with any material that can be charged, including organic and inorganic, metallic, semiconducting, and insulating materials. An interesting focusing effect has been observed that shows assembly at a resolution greater than the underlying pattern. The lateral placement accuracy, currently 25 nm standard deviation for the evaporation system, is defined by the level of control of the focusing effect as well as the minimal feature size of the underlying patterns, presently 100 nm. The resist does not carry particles in a belt surrounding the patterns. The size of the empty resist areas depends on the ratio between local and global field strength and has been larger than 10 μm. The process offers self-aligned integration and could be applied to integrate single-crystal silicon nanoparticle transistors[2] or other nanomaterial devices on desired areas on a surface. It could also be extended to externally biased surface electrodes that could be programmed to enable the integration of more than one material type.

Acknowledgment. We thank Dr. Uwe Kortshagen and Patrizio Cernetti for use of their silicon nanoparticle plasma system. This research was directly supported by NSF DMI-0556161 and NSF DMI-0621137. We also acknowledge NSF MRSEC Award DMR-0212302, ECS-0229097, and NIRT-0304211 for early seed support.

References

(1) Devoret, M. H.; Schoelkopf, R. J. **2000**, *406*, 1039−1046.
(2) Ding, Y.; Dong, Y.; Campbell, S. A.; Jacobs, H. O.; Bapat, A.; Kortshagen, U.; Perrey, C.; Carter, C. B. *Proceedings of 2005 NSF DMII Grantees Conference, Scottsdale, Arizona, January 3−6, 2005.*
(3) Xiang, J.; Lu, W.; Hu, Y.; Wu, Y.; Yan, H.; Lieber, C. M. *Nature* **2006**, *441*, 489−493.
(4) Fafard, S.; Hinzer, K.; Raymond, S.; Dion, M.; McCaffrey, J.; Feng, Y.; Charbonneau, S. *Science* **1996**, *274*, 1350−1353.
(5) Patolsky, F.; Zheng, G.; Lieber, C. M. *Anal. Chem.* **2006**, *78*, 4260−4269.
(6) Law, M.; Sirbuly, D. J.; Johnson, J. C.; Goldberger, J.; Saykally, R. J.; Yang, P. *Science* **2004**, *305*, 1269−1273.
(7) Brune, H.; Giovannini, M.; Bromann, K.; Kern, K. *Nature* **1998**, *394*, 451−453.
(8) Xia, Y.; Yin, Y.; Lu, Y.; McLellan, J. *Adv. Funct. Mater.* **2003**, *13*, 907−918.

(9) Cui, Y.; Bjoerk, M. T.; Liddle, J. A.; Soennichsen, C.; Boussert, B.; Alivisatos, A. P. *Nano Lett.* **2004**, *4*, 1093−1098.
(10) Kimura, K.; Yao, H.; Sato, S. *Synth. React. Inorg. Met.-Org. Nano-Met. Chem.* **2006**, *36*, 237−264.
(11) Yellen, B. B.; Friedman, G. *Adv. Mater.* **2004**, *16*, 111−115.
(12) Li, D.; Ouyang, G.; McCann, J. T.; Xia, Y. *Nano Lett.* **2005**, *5*, 913−916.
(13) Duan, X.; Huang, Y.; Cui, Y.; Wang, J.; Lieber, C. M. *Nature* **2001**, *409*, 66−69.
(14) Jacobs, H. O.; Barry, C. Method and Apparatus for Depositing Charge and/or Nanoparticles. U.S. Patent 2005123687, 2005.
(15) Jacobs, H. O.; Whitesides, G. M. *Science* **2001**, *291*, 1763−1766.
(16) Barry, C. R.; Lwin, N. Z.; Zheng, W.; Jacobs, H. O. *Appl. Phys. Lett.* **2003**, *83*, 5527−5529.
(17) Barry, C. R.; Gu, J.; Jacobs, H. O. *Nano Lett.* **2005**, *5*, 2078−2084.
(18) Krinke, T. J.; Fissan, H.; Deppert, K.; Magnusson, M. H.; Samuelson, L. *Appl. Phys. Lett.* **2001**, *78*, 3708−3710.
(19) Mesquida, P.; Stemmer, A. *Adv. Mater. (Weinheim, Ger.)* **2001**, *13*, 1395−1398.
(20) Naujoks, N.; Stemmer, A. *Microelectron. Eng.* **2005**, *78*−*79*, 331−337.
(21) Fudouzi, H.; Kobayashi, M.; Shinya, N. *J. Nanopart. Res.* **2001**, *3*, 193−200.
(22) Welle, A. M.; Jacobs, H. O. *Appl. Phys. Lett.* **2005**, *87*, 263119.
(23) Bapat, A.; Perrey, C. R.; Campbell, S. A.; Carter, C. B.; Kortshagen, U. *J. Appl. Phys.* **2003**, *94*, 1969−1974.
(24) Jacobs, H. O.; Stemmer, A. *Surf. Interface Anal.* **1999**, *27*, 361−367.
(25) Jacobs, H. O.; Knapp, H. F.; Muller, S.; Stemmer, A. *Ultramicroscopy* **1997**, *69*, 39−49.
(26) Whitby, K. T. *Rev. Sci. Instrum.* **1961**, *32*, 1351−1355.
(27) Romay, F. J.; Liu, B. Y. H.; Pui, D. Y. H. *Aerosol Sci. Technol.* **1994**, *20*, 31−41.
(28) Dong, Y.; Bapat, A.; Hilchie, S.; Kortshagen, U.; Campbell, S. A. *J. Vac. Sci. Technol., B* **2004**, *44*, 1923−1930.
(29) Schiel, A.; Weber, A. P.; Kasper, G.; Schmid, H.-J. *Part. Part. Syst. Charact.* **2002**, *19*, 410−418.
(30) Liu, B. Y. H.; Pui, D. Y. H.; Lin, B. Y. *Part. Part. Syst. Charact.* **1986**, *3*, 111−116.

NL0618703